J Mater Sci: Mater Electron

Investigation of the structural, magnetic, and cooling performance of AlFe thin film and AlFeGd nanometric giant magnetocaloric thin films

Suat Pat[1,*], Özgür Bayer[2], Sertan Kemal Akay[3], Reza Mohammadigharehbagh[3], and Metin Kaya[4]

[1] Faculty of Art and Letters, Physics Department, Eskişehir Osmangazi University, Eskişehir, Turkey
[2] Department of Mechanical Engineering, Middle East Technical University, Ankara, Turkey
[3] Physics Department, Uludağ University, Bursa, Turkey
[4] Arçelik A.Ş. Refrigerator Plant, Eskisehir, Turkey

Received: 5 November 2020
Accepted: 7 January 2021

© The Author(s), under exclusive licence to Springer Science+Business Media, LLC part of Springer Nature 2021

ABSTRACT

Giant magnetocaloric thin films are promising materials for new generation energy-efficient cooling systems. To investigate the cooling performance of AlFe and AlFeGd alloys, thin films have been deposited onto a glass substrate by thermionic vacuum arc (TVA) deposition system. TVA is a physical vapor deposition technology; it works in high vacuum and low-temperature conditions. AlFe and AlFeGd thin films are of significant importance for giant magnetocaloric materials. The surface and magnetic properties of a magnetic material are strongly dependent on the deposition process. In this paper, the structural, magnetic, and cooling performances of AlFe alloys with and without the Gd element have been investigated. When the Gd elements are added to AlFe alloys, the size of crystallite and the surface morphology of the giant nanometric magnetocaloric thin films are altered. The size of crystallite decreases to a lower value due to the Gd element added. According to the results of the elemental analysis, the elemental ratios of the AlFe and AlFeGd thin films were measured as (87:13) and (84:4:12), respectively, which are different from the ones reported previously. Magnetic cooling performance and magnetization strongly depend on these ratios. The mean values of crystallite size for the AlFe thin film and AlFeGd nanometric giant magnetocaloric thin film were measured as 50 nm and 12 nm, respectively. Following the Curie temperature of AlFeGd thin film, and the temperature difference it produces in the studied magnetic fields, 60 successive units of this material are assumed to form a magnetic refrigeration cycle. The coefficient of performance of this cycle is calculated to be 2.084—nearly two times better than the suggested cascade vapor-compression cycles in the same temperature range. This fact alongside the solid-state and environmentally friendly attributes of magnetic refrigeration

Address correspondence to E-mail: suatpat@ogu.edu.tr

https://doi.org/10.1007/s10854-021-05285-y
Published online: 02 February 2021

cycles makes the AlFeGd thin films a strong candidate for accomplishing an efficient refrigeration system.

1 Introduction

Burning fossil fuels and using traditional methods of refrigeration have led to global warming and ozone layer depletion [1, 2]. According to these reasons alongside other complications such as the technical limitations of vapor refrigeration systems, scientists and engineers have tried to stretch their strides in terms of finding new and more efficient ways of refrigeration, one of which is utilizing magnetocaloric effect [3]. In addition to the magnetic induction heating or cooling being a promising green technology, it is also considered to be a solid-state technology for cooling systems. Fe alloys such as La-Fe-Si [4], $AlFe_2B_2$ [5], Fe_2P [6], $Gd_{60}Fe_{20}Al_{20}$ [7], Fe-B-Cr-Ce [8], and Fe-Nb-B [9] show magnetocaloric or giant magnetocaloric (GM) property. These alloys can be used in cooling systems or refrigerators, as well as in different applications, namely, biosensors, smart implants, etc. The GM property strongly depends on the electronic configuration of the alloys. Other promising material is AlFeGd ternary magnetocaloric material. Magnetocaloric alloys can be deposited as thin films onto physical vapor deposition systems to form magnetocaloric devices to deposit nanometric giant magnetocaloric thin films (NMGMTF). It is well established that substrate materials can change the thin film properties drastically. Compared to the available values in the literature [10], nanoscale thin films (TF) affect the entropy change according to the bulk material. Therefore, it is hoped that NMGMTFs will open a new venue for the cooling/heating applications. NMGMTFs have been deposited by a physical vapor deposition technology, because thin film's surface area will be bigger than the bulk material. It is known that nanometric structure increases the device performance [2]. Since nanomaterials and nanosystems have different magnetocaloric properties according to their bulk forms, NMGMTF is a potential solution that might have the highest coefficient of performance (COP) in a refrigeration system. To reach this aim, an active surface is needed. An active surface must have roughness in the nanoscale level and all crystallites must be nearly the same over the coated surface.

The AlFeGd alloy is already reported as magnetocaloric material. It was noticed that the magnetic properties of this ternary alloy are strongly affected by the Fe amount in the structure. In a specified temperature interval, these types of systems have superparamagnetic properties along with the ferromagnetic group. For instance, the magnetothermal effect in the Fe-Al binary alloys is demonstrated due to spin density waves [9]. As of the best of our knowledge, adding Gd into the binary alloy leads to an increase in magnetic groups, afterward a larger moment, and finally an increase in magnetocaloric value in the AlFeGd ternary compound [11]. Burzo showed the deviation in the Fe magnetization due to substitution by Al in the iron 3d state [11]. It means that an increase in Al content causes a decrease in Fe effective moments. In a study by Xiong et al. [12], the largest magnetic entropy value for this ternary system has reached as high as 8.4 J/kgK. They declared this value due to Fe substitution by Al: a decrease in the value coincides with the increase in the Fe and Curie temperatures. In the work carried out by Fang and his co-worker [13], the Fe/Al ratio increase resulted in change of magnetic entropy from 2.92 to 5.01 J/kgK. The maximum magnetic entropy change was recorded as 7.14 J/kgK for the field intensity change between 0 and 5 T. The Curie temperature of 149K for the $Al_{20}Fe_{10}Gd_{70}$ system was reported. Also, the refrigerant capacity (RC) value was 532–780 J/kg in the range of the magnetic field mentioned. In this work, the system was suggested for a magnetic refrigerant application [14]. It is worth mentioning that the Curie temperature plays a major role in the performance characteristics of a magnetic refrigeration (MR) system. At the Curie temperature, the dM/dT curve for a particular material reaches a minimum [15]. Additionally, the maximum entropy change at the Curie temperature has been directly compared among different materials to investigate the cooling effectiveness of a particular material [16].

In this paper, AlFe thin film (TF) and AlFeGd NMGMTF which have very low Fe ratios (< 0.13) compared to Al (> 0.84) (non-magnetic material) ratios were deposited onto glass substrates by thermionic vacum arc (TVA) coating system. To

increase the magnetic properties, Fe and Gd were added. To determine the performance, the surface properties, crystallite size, surface characteristics, chemical composition measurements, magnetic properties measurements, thermodynamic calculations, and temperature measurements were carried out. For the characterization of the surface and microstructural properties; atomic force microscopy (AFM), field emission scanning electron microscopy (FESEM) and energy dispersive X-ray spectroscopy (EDX) were used. The adiabatic temperature change (ΔT) was measured directly by using a contactless optical temperature measurement system. In the literature, thermodynamic analyses of various materials have been studied and corresponding thermodynamic cycles were carried out by calculating the entropy differences [17, 18] by employing different methods. In this work, the performance of an MR Carnot cycle has been compared with the coefficient of performance (COP) values of a real vapor-compression cascade cycle.

2 Methodology

2.1 Experiments

Other coating technologies do not yet present the crystallite size distribution function for a coated layer. However, this function -similar to the Gauss distribution function- is determined only in TVA coating technology. TVA, a physical vapor deposition technology, using the binary AlFe thin film and ternary AlFeGd for the giant magnetocaloric alloys has been investigated in this work for evaluating the giant magnetocaloric effect. AlFe TF and AlFeGd NMGMTF have been deposited onto a microscope slide substrate by a TVA system. Gd and Fe slugs and pieces were purchased from a commercial trade firm (Alfa Aesar) and Al was purchased from a local manufacturer. The high purity (> 99%) materials were used in thin film deposition process. AlFe and AlFeGd materials are also known as alloys. Gd is a special element for magnetic investigations. TVA is a rapid vacuum plasma coating method that works in a high vacuum condition and it is producing high purity nano structured thin films [19–24]. TVA has two electrodes: anode and cathode. The anode is a tungsten evaporation boat, and the cathode is an electron gun, including a wolfram filament with diameter of 500 μm. The AlFe and AlFeGd alloys were placed into the evaporation boat. All depositions were realized at high vacuum conditions. For the deposition of the films, firstly electron gun was heated by a high current of 20 A. Then, a high voltage of 600 V was applied into inner electrodic space. Firstly, located Al: Fe and Al: Fe:Gd materials were melted by accelerated electrons with high DC voltage, then bright discharges were generated and glass substrates were coated by the materials plasma. In Fig. 1, the photo images of the AlFe and AlFeGd thin films coated glass are shown. All dimensions are in cm.

Before the ignition of plasma, the discharge current is in order of μA and after the ignition of plasma, the current was measured as 300 mA. Before the deposition process, glass substrates were cleaned by an ultrasonic bath and ethyl alcohol. Then, the glass substrates were dried by hot air before putting on the substrate holder for about 1–2 minutes. The surface temperature of the glass substrates in coating process was nearly at room temperature. TVA is also a green technology. In this process for the AlFe and AlFeGd thin films, no waste was produced. The TVA deposition parameters are summarized in Table 1. All samples are trimmed to 4 mm x 4 mm. The resistance for 10 mm length of AlFe and AlFeGd thin films is measured as 42 Ω and 67 Ω, respectively.

2.2 Thermodynamic analysis

A magnetic refrigerator is typically comprised of a magnetic material, a system capable of magnetizing and demagnetizing, hot and cold heat exchangers,

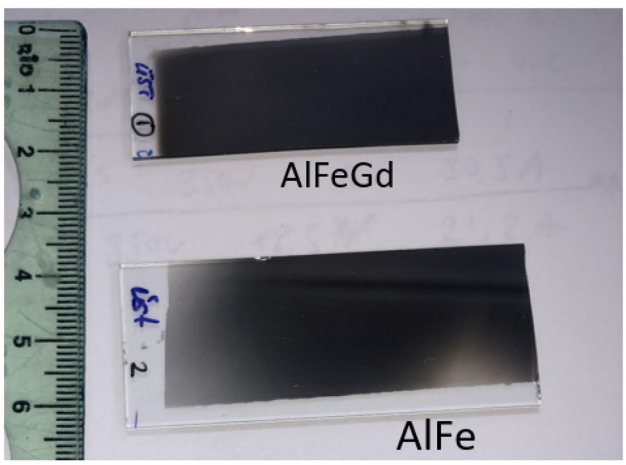


Fig. 1 The images of the AlFe and AlFeGd thin films

Table 1 TVA deposition parameters for AlFe and AlFeGd thin films

	Deposition pressure [mtor]	Filament current [A]	Filament voltage [V]	Applied voltage [V]	Discharge current [A]	Deposition time [s]
AlFe	9×10^{-5}	20	7.5	600	0.5	30
AlFeGd	8×10^{-5}				0.2	180

and a heat transfer system. In a magnetic refrigeration cycle, the working material is a solid-state magnetic material of that entropy and temperature change under the influence of a magnetic field. With the help of two processes of isothermal magnetization and adiabatic magnetization, a cyclic behavior can be achieved [25]. This section is divided into two subsections to illustrate the cyclic behavior of the MR at the experimental temperatures and introduce a comparison method with a real cascade vapor-compression cycle.

2.2.1 *Carnot refrigeration cycle analysis*

The MR cycle is assumed to be running ideally as a refrigeration system. A Carnot cycle is intended for thermodynamical modeling of the MR system. Figure 2 depicts the T-s diagram of the Carnot cycle.

The magnetic refrigerant is first partially magnetized (process 1–2). This process increases its temperature from T_{cold} to T_{hot} adiabatically. At the next step (process 2–3), the magnetic field is further increased isothermally to enable the working fluid in the heat exchanger to absorb the heat from the system. In the next process (process 3–4), the magnetic field which is applied to the system is decreased, which eventuates the temperature of the system to reach T_{cold} from T_{hot}. Then, the cycle is completed when the material is totally demagnetized in the last process (process $4-1$) in which the magnetic material absorbs heat from heat exchanger fluid [2, 25].

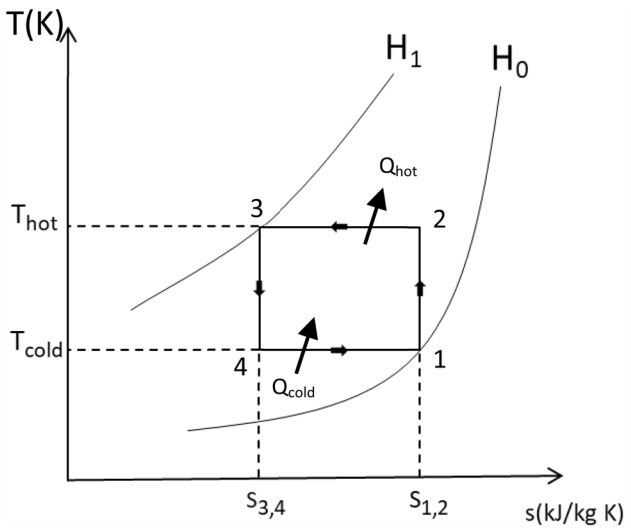


Fig. 2 T-s diagram of the MR Carnot cycle

The goal of this section is to measure and calculate the values pertinent to the Carnot cycle. Two different magnetic intensities 0.51 T and 2.6 T are designated to H_0 and H_1, respectively. In a thermodynamic Carnot cycle, the amount of net cooling capacity is defined as follows:

$$Q_{cold} = \Delta s_{1,4} T_{cold} \tag{1}$$

On the other hand, the net heat rejected is specified as follows:

$$Q_{hot} = \Delta s_{3,2} T_{hot} \tag{2}$$

These values lead to the calculation of input work by employing the first law of thermodynamics as follows:

$$W = Q_{hot} - Q_{cold} \tag{3}$$

The COP of the Carnot MR cycle is defined as the ratio of net cooling capacity to the input work. Since the amount of entropy change is the same for both input work and net cooling capacity in an ideal Carnot cycle, the COP of the system reduces as follows:

$$COP_{MR} = \frac{Q_{cold}}{Q_{hot} - Q_{cold}} = \frac{T_{cold}}{T_{hot} - T_{cold}} \tag{4}$$

2.2.2 *Cascade refrigeration cycle comparison*

Applications employing refrigeration include vast areas of modern world. The refrigeration temperature, besides playing role in defining the application,

spans broadly in its value. The basic vapor-compression cycle (VCC) covers the most common application due to its flexible refrigeration temperature and the availability, low cost, and maintenance requirements [26]. One disadvantage of VCC is its limiting minimum refrigeration temperature which hovers around − 40 °C (233K) [27]. For compensation, cascade cycles are introduced so that a refrigeration temperature between 120K and 233K would be provided [26]. In cascade cycles, usually, two separate VCCs are designed over each other and coupled through the cascade condenser as shown in Fig. 3 to reach the desired temperature.

Cascade cycles are commonly used in applications in which a quick-freezing process is required such as food freezing [28]. Other uses of VCC refrigeration cycles include some industrial utilizations such as liquefaction of gases and biological materials [29]. A cascade cycle T-s diagram is depicted in Fig. 4. Although the MR Carnot cycle represents an ideal process, by comparing the COP of these cycles, a comparison of the performances can be employed. The COP of the cascade cycle is defined as the ratio of the net cooling capacity of the evaporator, Q_e to the work inputs, $W_{comp,LTC}$ and $W_{comp,HTC}$, of the low- and high-temperature compressors, in LTC and HTC [30]:

$$COP = \frac{Q_e}{W_{comp,LTC} + W_{comp,HTC}} \tag{5}$$

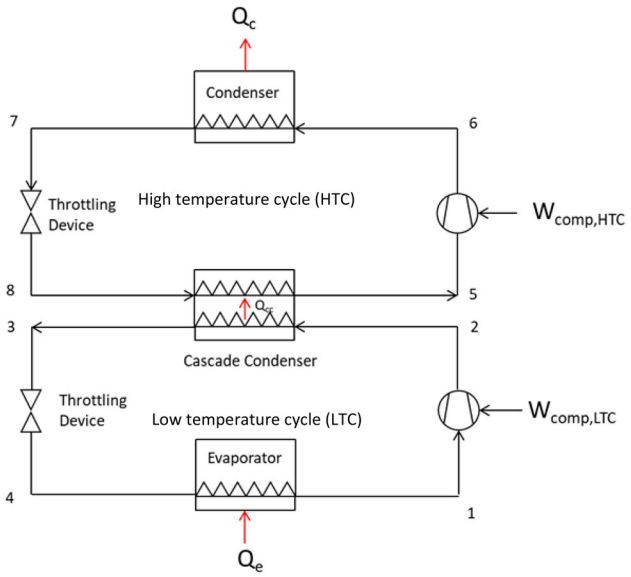


Fig. 3 A Schematic diagram of a cascade VCC

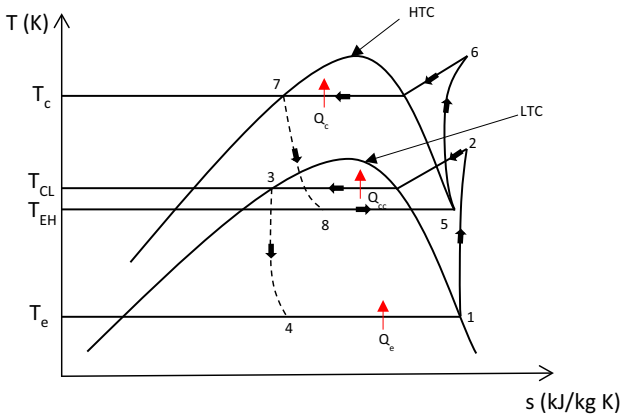


Fig. 4 T-s diagram of a cascade refrigeration cycle

3 Results and discussion

3.1 Surface analyses

To determine the surface properties of AlFe and AlFeGd thin films, deposited thin films were investigated by field emission scanning electron microscopy (FESEM) with energy dispersive X-ray spectroscopy (EDX) and atomic force microscopy (AFM) devices. As a FESEM device, Hitachi REGULUS 8230 SEM with COLD FEG was used for the surface analysis. FESEM images of the AlFe and AlFeGd alloys are available in Fig. 5a and b. White spots in Fig. 5b mark the Gd elements which are seen clearly over the surface and they are uniformly distributed. The crystallite size for the alloy with Gd is smaller than the ones without Gd. From the surface images, grains are seen and the effect of Gd elements on surface can clearly be observed. Ambios Q-Scope atomic force microscopy (AFM) was used for the 3D surface images analysis, grain size distribution, and surface characteristics. AFM images are shown in Fig. 5c and d. It is understood from Fig. 5a and d that the grain size of the AlFe thin film is greater than the crystallite of AlFeGd thin film. Therefore, scanning sizes of FESEM and AFM images must be different. AFM scan sizes for AlFe and AlFeGd are 10 µm x 10 µm and 6 µm x 6 µm, respectively. In Fig. 5d, grains are very small. Differences of the grains in AFM images are seen in Fig. 5c and d. The grain size from the Fig. 5c and d were measured as approximately 50 nm and 12 nm for AlFe and AlFeGd thin films, respectively.

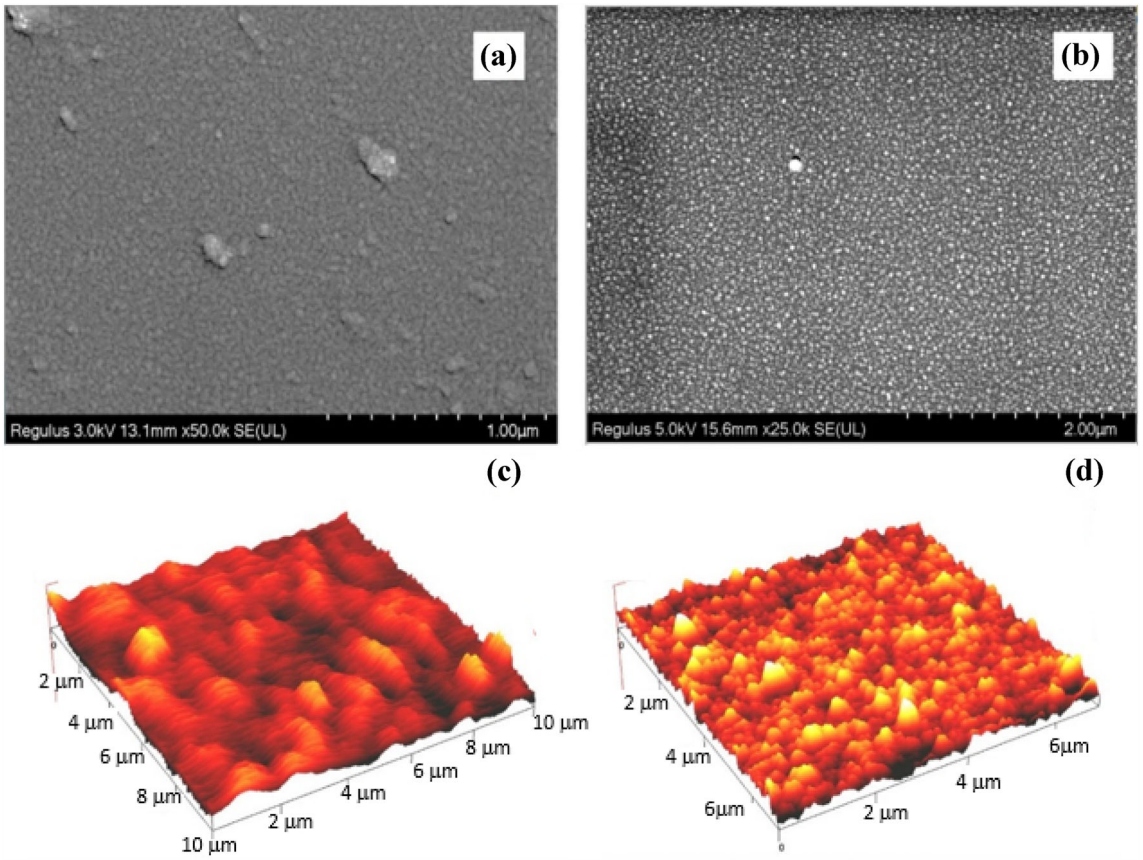


Fig. 5 **a** and **b** FESEM and **c** and **d** AFM images of AlFe and AlFeGd thin films

In Table 2, EDX results are presented. According to these results, the ratios of Al are close to each other. However, the ratio of Fe was decreased to 4 % from 13 % by the Gd element addition. The Gd ratio in AlFeGd NMGMTF was measured as 12 %. No Impurities were detected in the films. Other element ratios (O, Na and Si) came from the substrate material and they were removed from the table.

3.2 Crystallite size analyses

Crystallite size distribution (CSD) functions of AlFe thin film and AlFeGd NMGMTF are illustrated in Fig. 6. CSDs were measured by AFM device in 10 μm x10 μm and 6 μm x6 μm scales. For an absolute uniform particle distribution of a coated surface, CSD plot is expected to be similar to the perfect Gaussian curve and the standard deviation of the Gaussian curve should be a minimum. Hence, a CSD graph gives the information about the crystallite sizes deposited onto any substrate. Mean values of CSD for

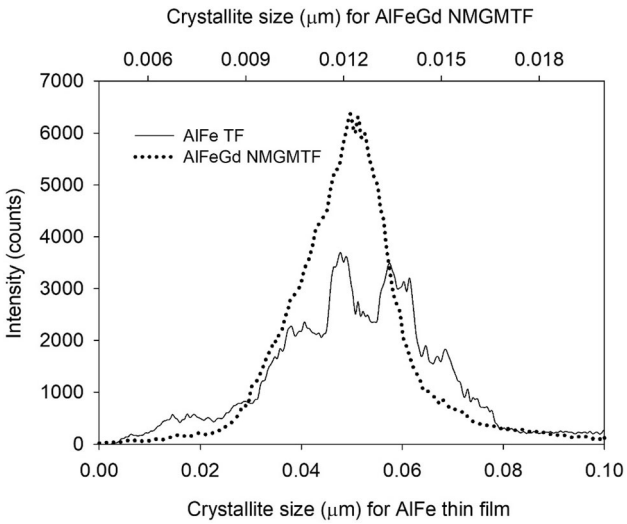


Fig. 6 Crystallite size distribution functions of the AlFe thin film and AlFeGd NMGMTF

Table 2 EDX analysis results of (a) AlFe and (b) AlFeGd thin films

Sample	Al	Fe	Gd	Total
AlFe	87	13	–	100
AlFeGd	84	4	12	100

the AlFe thin film and AlFeGd NMGMTF from the CSD graph are 50 nm and 12 nm, respectively. According to the CSD plot for the AlFe NMGMTF, different crystallite sizes were detected, while only one type of crystallites was detected for AlFeGd. Statistical data of the CSD plots are available in Table 3. The data (Ssk and Skr) are related to the shape of the Gauss distribution function of the CSD and gives the homogeneity of the particle over the film surface.

When the Gd elements are added to AlFe, it can be deducted from Fig. 6 that the size of crystallite is decreased, and the size distribution graph is even more homogeneously distributed. The mean value and the frequency are low compared to the AlFe case.

3.3 Magnetic measurements

Vibrating Sample Magnetometer (VSM) was used to measure the magnetic properties of the AlFe TF and AlFeGd NMGMTF. VSM-recorded graphs of the AlFe and AlFeGd NMGMTF are illustrated in Fig. 7a and the magnetization curve of the AlFeGd NMGTF is plotted in Fig. 7b. Some discrepancies between the magnetic properties of the AlFe TF and AlFeGd NMGMTF are observed. All measurements were done at room temperature and all deposited thin films were directly measured without any heat treatment. M (emu) -H (Oe) curve for AlFe thin film almost looks like a straight line similar to a diamagnetic material. The AlFeGd sample also demonstrates ferromagnetic properties. With the substitution of gadolinium elements (12 %) with iron element (9 %) for the AlFe thin film, the magnetic properties of the AlFeGd NMGMTF showed a ferromagnetic behavior as well. The thickness of the films was approximately 50 nm. The mass of NMGMTF deposited onto glass substrate was calculated as 10 ng. Therefore, M(emu/g) are very high compared to the literature.

Table 3 Statistic surface analyses data of the CSD plots

	AlFe	AlFeGd	Unit
Average height	59	12	nm
RMS deviation (Sq)	34	4	nm
Mean deviation (Sa)	20	2	nm
Max deviation	230	39	nm
Skewness (Ssk)	3	3.8	–
Kurtosis (Skr)	12	20.3	–

M(emu/g) is obtained bigger than the 1000 emu/g for the AlFeGd NMGMTF sample. Figure 7a reveals that the saturation regime for AlFeGd NMGMTF starts at approximately +1.2 kOe and − 1.2 kOe. In Fig. 7b, a hysteresis loop is illustrated for the AlFeGd NMGMTF sample. Consistent with the literature, increasing the Gd ratio decreased the crystallite sizes and saturation magnetization. Similar behavior is observed in the study by Yadav et al. [31]. Also, the atomic ratios, given in Table 2, were adjusted before the experiment. All these films were deposited in different batches. Al atomic ratio in the deposited thin films was kept nearly constant and for some, Fe atoms were substituted by Gd atoms.

The AlFe thin film showed a diamagnetic behavior with low negative magnetic moment by the applied magnetic field, as observed in Fig. 7a. After the substitution of some Gd atoms in place of Fe atoms, the diamagnetic behavior changed to ferromagnetic one. The saturation regime and ferromagnetic properties are seen clearly in Fig. 7b for AlFeGd NMGMTF. The diamagnetic properties of the glass substrate are dominant after the saturation regime. The obtained results are in a very good agreement with the ones in [32], providing an independent confirmation of the yields reported in this study.

3.4 COP comparison

Since the Curie temperature of the studied material is around 200K, to achieve the highest entropy change—and consequently highest refrigeration capacity—the lowest temperature of the LTC, the evaporator (T_{cold}) temperature, is designated to be the Curie temperature (200K) and the HTC's highest temperature (T_{hot}) is designated to be the room temperature (296K). To achieve this temperature difference, it is assumed that 60 units of AlFeGd films are ordered in a series manner and the COP of the Carnot cycle is calculated according to Eq. 4.

In the literature, a vast temperature range for cascade VCCs are available [29, 33, 34]. Various cycles were analyzed to investigate the effect of various parameters. Most of the studies consider variation of refrigerants in LTC and HTC. In these studies, Tc usually sits above the one taken in the current study. However, it is noticeable that the COPs of these cycles are smaller when compared to the introduced MR cycle.

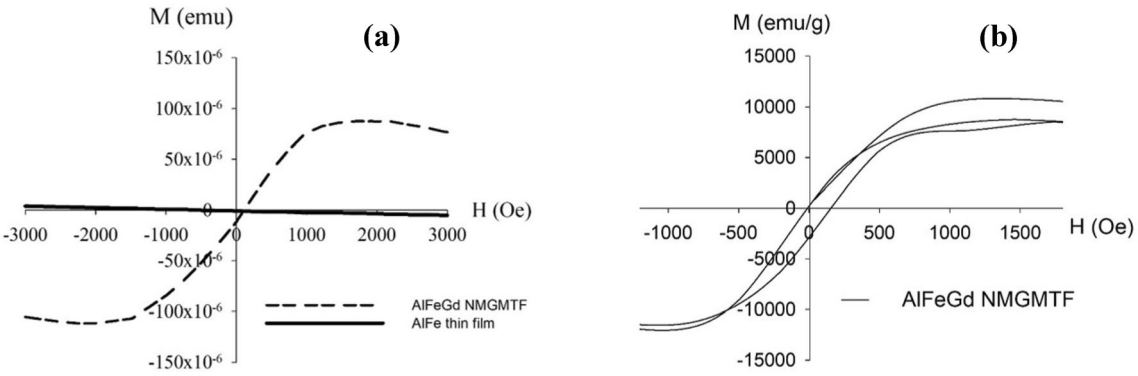


Fig. 7 **a** The VSM-recorded graphs of the AlFe TF and AlFeGd NMGMTF and **b** the magnetization curve of the AlFeGd NMGTF

To draw a clearer picture for the COP comparison of the proposed MR cycle with the cascade VCCs available in the literature, the closest T_c and T_e temperatures are chosen. The results are depicted in Table 4, which indicates that a MR Carnot cycle performs superiorly in terms of COP since it is an ideal cycle. Additionally, this advantage comes with some attractive features like being a green refrigeration system, having low-maintenance requirement, and solid-state nature of the system.

4 Conclusions

AlFe and AlFeGd alloys are promising materials for the effective and high-performance cooling systems. For this reason, these ternary compound alloys have been actively investigated by the researchers for industrial applications. Especially, thin films and nanometric structures show notable magnetic properties and enhance the capability of entropy change of the material. The dimensions of the investigated AlFe thin film and AlFeGd nanometric giant magnetocaloric thin films (NMGMTF) are 4 mmx 4 mm and the thickness of the AlFe and AlFeGd layer of 50 nm coated glass sample is 1 mm.

Table 4 Comparison of COP between MR Carnot cycle and cascade VCCs

Study	T_e [K]	T_c [K]	Refrigerants	COP
Parekh and Tailor [35]	191	298	R507A-R23	0.925
Parekh and Tailor [36]	200	298	R12-R13	1.335
			R404A-R23	1.335
			R290-R13	1.361
Gami and Aijaz [37]	200	308	R290-R23	0.855
			R134a-R23	0.862
Current study	200	296	–	2.084

The chemical composition of the AlFe thin film and AlFeGd NMGMTF are determined as (87:13) and (84:4:12), respectively. 12% Gd change in the alloy affects the surface properties, crystallite sizes, and magnetocaloric properties drastically. Mean crystallite size of AlFeGd NMGMTF is 12 nm and this sample shows notable performance in the present application.

Although it was mentioned that the maximum refrigeration capacity can be extracted near the Curie temperature, the experiments, in this study, were carried out at room temperature and the Carnot cycle T-s diagram was presented. Investigation of AlFeGd thin films resulted in 1.6 ºC difference when subjected to a magnetic field. An assumption of a system in which a series of 60 units of AlFeGd are successively considered were modeled as a Carnot cycle and its COP was calculated. When compared to available cascade vapor-compression cycles in the similar temperature range, the ideal MR cycle resulted in approximately 55%, up to more than two times better performance depending on the refrigerant and working temperatures of available cascade vapor-compression cycle.

It is concluded that the utilization of AlFeGd-based thin films has a great potential in refrigeration especially when a fast and relatively low refrigeration temperature is required. In the future works, by modeling a more realistic cycle such as a Brayton cycle, it is hoped that this system will be understood more deeply. Additionally, the calculation of maximum entropy difference at the Curie temperature

will be carried out to give a better outline of the refrigeration potential. Consequently, AlFeGd NMGMTF is a promising material for cooling application.

References

1. J.U. Ahamed, R. Saidur, H.H. Masjuki, Renew. Sustain. Energy Rev. (2011). https://doi.org/10.1016/j.rser.2010.11.039
2. V. Franco, J.S. Blázquez, J.J. Ipus, J.Y. Law, L.M. Moreno-Ramírez, A. Conde, Prog. Mater Sci. (2018). https://doi.org/10.1016/j.rser.2010.11.039
3. J. Romero Gómez, R. Ferreiro Garcia, A. De Miguel Catoira, M. Romero, Gómez, Renew. Sustain. Energy Rev. (2013). https://doi.org/10.1016/j.rser.2012.09.027
4. J. Lyubina, O. Gutfleisch, M.D. Kuz'min, M. Richter, J. Magn. Magn. Mater. (2009). https://doi.org/10.1016/j.jmmm.2008.04.116
5. J.W. Lee, M.S. Song, B.K. Cho, C. Nam, Curr. Appl. Phys. (2019). https://doi.org/10.1016/j.cap.2019.05.004
6. L. Caron, M. Hudl, V. Höglin, N.H. Dung, C.P. Gomez, M. Sahlberg, E. Brück, Y. Andersson, P. Nordblad, Phys. Rev. B - Condens. Matter Mater. Phys. (2013). https://doi.org/10.1103/PhysRevB.88.094440
7. N.T.M. Duc, H.X. Shen, E.M. Clements, O. Thiabgoh, J.S. Llamazares, C.F. Sanchez-Valdes, M.H. Phan, J. Alloys Compd. **807**, 151694 (2019).
8. J.Y. Law, V. Franco, R.V. Ramanujan, J. Appl. Phys. (2011). https://doi.org/10.1063/1.3613666
9. S.G. Min, K.S. Kim, S.C. Yu, K.W. Lee, Mater. Sci. Eng. A (2007). https://doi.org/10.1016/j.msea.2006.02.357
10. C.W. Miller, D.D. Belyea, B.J. Kirby, J. Vac. Sci. Technol. A Vacuum, Surfaces, Film. (2014). https://doi.org/10.1116/1.4882858
11. E. Burzo, J. Phys. F Met. Phys. (1980). https://doi.org/10.1088/0305-4608/10/9/018
12. D.K. Xiong, D. Li, W. Liu, Z.D. Zhang, Phys. B Condens. Matter (2005). https://doi.org/10.1016/j.physb.2005.08.026
13. Y.K. Fang, H.C. Chen, C.C. Hsieh, H.W. Chang, X.G. Zhao, W.C. Chang, W. Li, J. Appl. Phys. (2011). https://doi.org/10.1063/1.3561447
14. Z. Zheng, X. Zhong, K. Su, H. Yu, Z. Liu, D. Zeng, Sci. China Physics, Mech. Astron. (2011). https://doi.org/10.1007/s11433-011-4363-4
15. S. Kallel, N. Kallel, O. Peña, M. Oumezzine, Mater. Lett. (2010). https://doi.org/10.1016/j.matlet.2010.02.005
16. A. Kitanovski, P.W. Egolf, J. Magn. Magn. Mater. (2009). https://doi.org/10.1016/j.jmmm.2008.11.078
17. G. Diguet, G. Lin, J. Chen, Int. J. Refrig. (2013). https://doi.org/10.1016/j.ijrefrig.2012.11.022
18. G. Diguet, G. Lin, J. Chen, Int. J. Refrig. (2012). https://doi.org/10.1016/j.ijrefrig.2011.12.004
19. A. Olkun, S. Pat, N. Akkurt, R. Mohammadigharehbagh, U. Demirkol, M. Özgür, Ş Korkmaz, J. Mater. Sci. Mater. Electron. (2020). https://doi.org/10.1007/s10854-020-04444-x
20. N. Akkurt, S. Pat, R. Mohammadigharehbagh, M. Özgür, U. Demirkol, A. Olkun, Ş Korkmaz, J. Mater. Sci. Mater. Electron. (2020). https://doi.org/10.1007/s10854-020-03499-0
21. S. Elmas, S. Pat, R. Mohammadigharehbagh, C. Musaoğlu, M. Özgür, U. Demirkol, S. Özen, Ş Korkmaz, Phys. B Condens. Matter (2019). https://doi.org/10.1016/j.physb.2019.05.035
22. C. Musaoğlu, S. Pat, R. Mohammadigharehbagh, S. Özen, Ş Korkmaz, J. Electron. Mater. (2019). https://doi.org/10.1007/s11664-018-06906-9
23. S. Elmas, S. Pat, R. Mohammadigharehbagh, C. Musaoğlu, M. Özgür, U. Demirkol, S. Özen, Ş Korkmaz, Phys. B Condens. Matter (2019). https://doi.org/10.1016/j.physb.2018.12.039
24. M. Özgür, S. Pat, R. Mohammadigharehbagh, C. Musaoğlu, U. Demirkol, S. Elmas, S. Özen, Ş Korkmaz, J. Alloys Compd. (2019). https://doi.org/10.1016/j.jallcom.2018.10.020
25. V. Basso, C.P. Sasso, G. Bertotti, M. LoBue, Int. J. Refrig. (2006). https://doi.org/10.1016/j.ijrefrig.2005.04.007
26. V.S. Chakravarthy, R.K. Shah, G. Venkatarathnam, J. Therm. Sci. Eng. Appl. (2011). https://doi.org/10.1115/1.4003701
27. A.S. Dalkilic, S. Wongwises, Int. Commun. Heat Mass Transf. (2010). https://doi.org/10.1016/j.icheatmasstransfer.2010.07.006
28. C.R. Taylor, ASHRAE J. **44**, 9 (2002).
29. Y. Ust, A.S. Karakurt, Arab. J. Sci. Eng. (2014). https://doi.org/10.1007/s13369-014-1335-9
30. M.J. Moran, H.N. Shapiro, Fundamentals of Engineering Thermodynamics, 9th edn. (Wiley,2018), p. 383
31. R.S. Yadav, I. Kuřitka, J. Vilcakova, J. Havlica, L. Kalina, P. Urbánek, M. Machovsky, D. Skoda, M. Masař, J. Mater. Sci. Mater. Electron. (2018).https://doi.org/10.1007/s10854-018-9674-z
32. J. Shah, R.K. Kotnala, J. Mater. Chem. A (2013). https://doi.org/10.1039/C3TA11845B
33. Y. Xie, C. Liu, L. Lun, X. Zhang, Int. Refrig. Air Cond. Conf. Pap. 939. (2008)
34 P.L. Rupesh, J.M. Babu, D. Surryaprakash, R.D. Misra, *Int* (Smart Technol. Manag. Comput. Commun. Control. Energy

Mater, Conf, 2015). https://doi.org/10.1109/ICSTM.2015.7225494
35. A.D. Parekh, P.R. Tailor, Int. J. Mech. Mechatronics Eng. (2011). https://doi.org/10.5281/zenodo.1054847
36. A.D. Parekh, P.R. Tailor, Int. J. Mech. Mechatronics Eng. (2014). https://doi.org/10.5281/zenodo.1337357
37. H.M. Gami, M.A. Ajazi, Int. J. Eng. Sci. Res. Technol. **3**, 4 (2017).

Publisher's note Springer Nature remains neutral with regard to jurisdictional claims in published maps and institutional affiliations.